Measurement of microbubble-induced acoustic microstreaming using micro particle image velocimetry

Paul Tho[a], Yonggang Zhu[b], Richard Manasseh[b], Andrew Ooi[a]

[a]Department of Mechanical and Manufacturing Engineering, The University of Melbourne, Parkville, Victoria 3010, Australia
[b]Energy and Thermofluids Engineering, CSIRO Manufacturing and Infrastructure Technology, Highett, Victoria 3192, Australia

ABSTRACT

Micro particle image velocimetry (PIV) measurements of the velocity fields around oscillating gas bubbles in microfluidic geometries were undertaken. Two sets of experiments were performed. The first measured the acoustic microstreaming around a gas bubble with a radius of 195 μm attached to a wall in a chamber of 30 mm× 30 mm× 0.66 mm. Under acoustic excitation, vigorous streaming in the form of a circulation around on the bubble was observed. The streaming flow was highest near the surface of the bubble with velocities around 1mm/s measured. The velocity magnitude decreased rapidly with increasing distance from the bubble. The velocity field determined by micro-PIV matched the streaklines of the fluorescent particles very well. The second set of experiments measured the streaming at the interface between a trapped air bubble and water inside a microchannel of cross section 100 μm × 90 μm. The streaming flow was limited to within a short distance from the interface and was observed as a looping flow, moving towards the interface from the top and being circulated back from the bottom of the channel. The characteristic streaming velocity was in the order of 100 μm/s.

Keywords: Micro-PIV, microfluidics, acoustic microstreaming, microbubbles

1. INTRODUCTION

The development of integrated microscale devices in recent years using micro-electromechanical systems (MEMS) technology has brought with it a demand to study flow behaviour and develop systems with characteristic dimensions less than 1 mm. Microfluidics in these devices has found a wide range of applications such as DNA hybridization assays[1], chemical microreactors[2], micro-fuel cells[3] and micro sensors[4].

The study of microfluidics has been greatly aided by the development of the micro particle image velocimetry (micro PIV) technique, an extension of the PIV technique commonly used in studies of macro scale flow[5]. The conventional PIV technique is unsuitable for use in microfluidic systems because of the limitations of its spatial resolution with respect to microfluidic length scales and the practical difficulty of accurately aligning a light sheet with the objective plane. The essential difference between a micro-PIV and a conventional PIV is the illumination. Conventional PIV uses a thin light sheet to define the imaging plane, while micro-PIV uses volume illumination and relies on the small depth of field of the microscope objective to define the imaging plane. The depth of field of an objective is governed strongly by its numerical aperture with larger numerical apertures providing smaller depths of field. The micro PIV technique has been well documented in a number of publications.[6,7,8,9,10]

Micro-PIV measurements have been performed on a number of different micro flow geometries. High spatially resolved velocity measurements in a microchannel of cross section 30 μm × 300 μm were taken by Meinhart et al[7]. In this experiment dual Nd:YAG lasers imaged 200 nm fluorescent polystyrene particles through a 60× magnification objective lens and a CCD camera. An ensemble average of the cross-correlation functions prior to peak detection ensured a high signal to noise ratio. The velocity vectors were within 2% of the analytical solution. Devasenathipathy et al.[8] measured

the flow field at the intersection of a cross channel system. The hydraulic diameter of the channel cross section was 66μm. The measured velocity results agreed well with numerical simulations and Particle Tracking Velocimetry (PTV) measurements. Meinhart and Zhang[9] also used a similar set up to study the flow inside the nozzle of an inkjet printhead. Flow velocities up to 8 m/s were measured using 700 nm fluorescent particles and a 40× objective lens. Their measurements showed the stages of droplet and meniscus formation inside the nozzle over a cycle of ejection. Kim et al[10] performed micro-PIV measurements in a Y-shaped microchannel in comparison to simulations to investigate the effect of different refractive indices of glycerol mixtures on velocity measurements. Their results show good agreement between the simulations and the measured velocity profiles.

The present study aims to measure the flow field due to acoustic microstreaming. The steady streaming flow induced by a bubble undergoing small amplitude periodic oscillations in a viscous fluid is known as acoustic microstreaming. The source of this flow is attributed to the Reynolds stresses generated inside the Stokes layer on the oscillating surface creating vorticity extending to the edge of this layer. This vorticity, essentially acting as an apparent slip velocity to the outer flow, extends outside the layer, thus driving the bulk fluid flow well beyond the Stokes layer. The thickness L of the Stokes layer is given in (1)[11].

$$L = \sqrt{\frac{2\nu}{\omega}}$$
(1)

Here ν is the kinematic viscosity of the fluid and ω is the frequency of oscillation.

Experimental observations of streaming around an oscillating bubble was first made in the 1950's by Kolb and Nyborg[12]. In their experiment a small air bubble was attached to a thin plastic film inside a clear cell. The bubble was excited by passing sound from a horn driver through an air channel to the thin plastic film. When the horn was activated, little activity was observed in the vicinity of the film without a bubble. However when a bubble formed or was placed on the surface of the film, vigorous eddying motions were observed. Similar work was carried out by Elder[13] who observed streaming motions around small bubbles inside a tank at different driving amplitudes and fluid viscosities. His work identified several stable regimes of streaming behaviour. More recently, Marmottant and Hilgenfeldt[14] have demonstrated that the shear forces developed around an oscillating bubble could be used as a means of cell wall permeation.

In a microfluidic context, acoustic microstreaming has been observed by Liu et al[15]. Air bubbles trapped in pockets inside a circular chamber 300 μm deep and 15 mm in diameter were excited and the streaming around the bubbles was observed as vortex motions using dyes. However, there is little quantitative information available about the flow field induced by the streaming. In this paper we will present two sets of micro-PIV measurements: the flow around an oscillating bubble between two plane walls and also the flow near the air-water interface formed between a slug of air trapped at the end of a closed channel and a drop of water.

2. EXPERIMENTAL SET UP

2.1. Micro-PIV system

The micro-PIV system at the CSIRO Microfluidics Laboratory, Melbourne (Figure 1) consists of an inverted epi-fluorescent microscope (Nikon TE2000-E), dual Nd:YAG lasers (New Wave, Minilase III) and a CCD camera imaging system (PCO Sensicam QE). The two laser beams were delivered into the microscope through an optical fibre and laser beam expander and then relayed through a fluorescent filter cube into the microfluidic device. The fluorescent filter cube contains three filters (Chroma Technology Corp): a 532 nm excitation filter (a notch filter), a dichroic beam splitter which transmits light above 550 nm and an emitter (barrier) filter transmitting light above 560 nm.
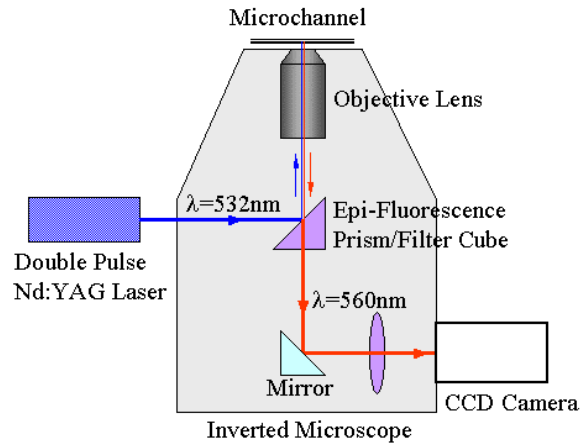
Figure 1: Set-up of the micro PIV system. A double pulsed Nd:YAG laser is used to illuminate 2 μm and 0.6 μm diameter fluorescent particles in the microchannel through an epi-fluorescent inverted microscope. A cooled 1376×1040 pixels, 12-bit interline-transfer CCD camera is used to record the particle images.

The seeding particles (Duke Scientific) for flow visualization and micro-PIV measurements are polystyrene spheres coated with a red fluorescent dye. The particles are nearly neutrally buoyant in water (specific gravity 1.05) and have a peak excitation at 542 nm and peak emission at 612 nm. Hence, the filtering arrangement just described passed only the light re-emitted by the particles to the camera, while removing direct reflections. Particles of diameter 2 μm and 0.6 μm were used in this set of experiments. These particle sizes were chosen so that the visibility and size of the particle image was distinguishable from the background while using as small particles as possible to ensure the particles followed the flow accurately. Ultimately these were dictated by the choice of objective magnification used. The particle seeding density for both experiments was approximately 0.025%(v/v).

The microscope objectives used were 4× and 40× Nikon CFI Plan Fluor objectives with numerical apertures of 0.13 and 0.6 respectively. Light collected from the objectives passes through the filter cube to the CCD camera (12 bit, 1376 x 1040 pixels). The images recorded were limited to a region of interest of 800 × 800 pixels. Illumination for micro-PIV measurements is with Nd:YAG lasers delivering 2 mJ, 532 nm laser pulses with a pulse width between 5-7 ns and a beam diameter 3.5 mm. A continuous 100 W super high pressure mercury arc lamp delivered through the filter cube was used for flow visualization purposes.

For each measurement, a pair of images was recorded with a specified time delay and the image recordings were synchronised with laser firings by an in-house built control circuit. The image pairs were processed using commercially available PIV software (VISIFLOW) to calculate velocity vectors. This method is based on the standard cross correlation algorithm. For each velocity measurements, fifty pairs of images were taken to obtain ensemble-averaged velocity data.

2.2. Bubble between two plane walls

Two sets of experiments were carried out. The first experiment measured the streaming generated by a sub-millimetre bubble attached to a wall. The system consists of a polycarbonate square cross sectional chamber (30 mm × 30 mm) with a depth of 0.66 mm (Figure 2). The depth of the chamber was determined by focusing on the bottom and upper walls of the chamber and measuring the relative change in microscope stage height via a *z*-axis reading with an uncertainty in the order of 2μm. A piezoelectric disk was attached centrally on the outer side of the upper wall. Oscillation of a bubble attached to the upper wall was induced by the 12 mm diameter PZT (lead zirconate titanate) disk (APC International). The PZT disk was attached with leads to a signal function generator (Wavetek model 145).

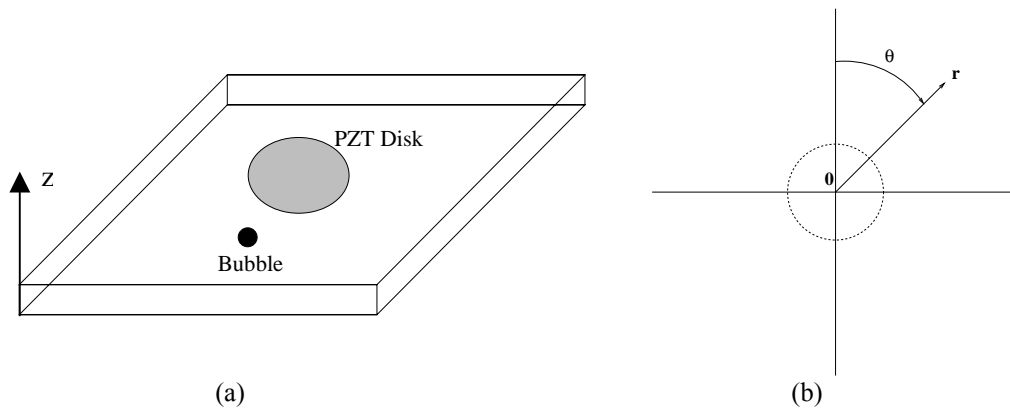<div align="center">(a)   (b)</div>

Figure 2: (a) Set-up of bubble streaming between two plane walls. Bubble and PZT disk are both placed on the top side of the chamber. (b) Polar coordinate system was used for this experiment with origin at the bubble centre.

2.3. Bubble in a microchannel

The second experiment investigated streaming near a water drop in a microchannel (Figure 3). The microchannel was made using a standard photolithography technique. In brief, the 2-D microchannel pattern was first designed using a computer drawing package. The pattern was then printed onto a transparency as a mask. The SU8 mould was made by spin-coating SU8 material (series 2035 from Microchem, MA, USA) onto a 4" silicon wafer (Silicon Quest International, Inc., Santa Clara, CA) and then exposed by UV light through the mask. After developing, a negative of the channel pattern was formed on the silicon substrate. Next, a 10+1 mixture of PDMS (polydimethylsiloxane) prepolymer and curing agent (Sylgard® 184 Silicon Elastomer from Dow Corning, USA) was cast over the mould with a frame for holding the solution and cured for 1 h at 65 °C. After curing, the PDMS replica was peeled from the mould and holes were punched on the PDMS replica as access ports. The PDMS replica was then sealed to a Pyrex glass slide by adhesion to make a microfluidic device. The total length of the channel is 1.25mm. The channel cross section was 100 μm in width and 90 μm in depth. The two liquid ports were linked to the channel via a double-T configuration. The distance between the two T crosses was 450μm. A 12 mm PZT disk was placed on the PDMS side of the microchannel and attached to a function generator.
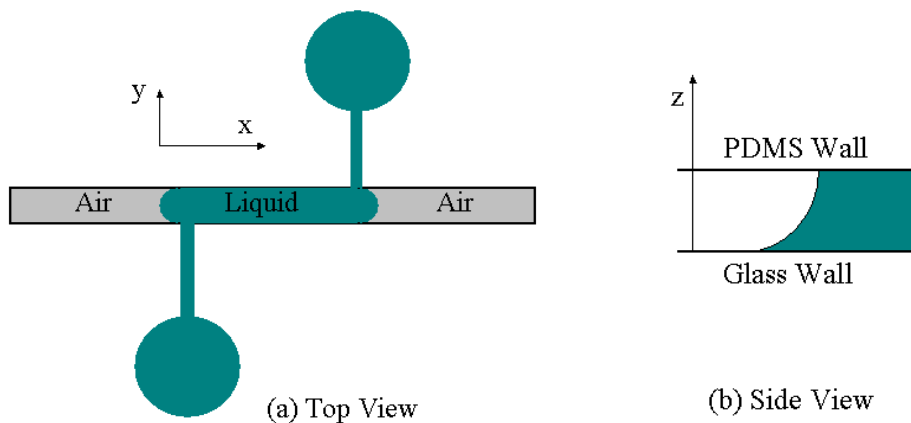

Figure 3 Set-up of bubble streaming in the microchannel and the corresponding coordinate system. The top view (a) shows the overall channel arrangement while the side view (b) shows the schematic of the air-water interface between the PDMS and glass walls. Due to the different contact angle of PDMS and glass materials with water, the interface is asymmetric with respect to the mid-place. The PZT disk was placed in the vicinity of the microchannel (not shown in the figure).

3. EXPERIMENTAL TECHNIQUE

3.1. Bubble between two plane walls

The chamber was filled with a solution of DI water and 2 μm seeding particles. A gas bubble (195 μm radius) was placed 4 mm from the edge of the PZT disk onto the upper inner wall using a syringe needle. A sinusoidal excitation signal was applied by the generator with a peak to peak voltage of 30 V and frequency of 291 Hz.

The 4× magnification objective lens was used to visualize the entire bubble and the surrounding flow field. The 2 μm particles were chosen as the seeding particles because smaller particles were difficult to resolve individually. The field of view from this objective lens was approximately 1.3 mm × 1.3 mm. Images were taken on a focal plane 75 μm from the base of the bubble.

The streaklines traced by the particles fully represent the streamlines of the flow field due to the steadiness of the flow. The streaklines were imaged using the 532 nm (green) filtered light from the mercury arc lamp passed through the filter block. The CCD camera's exposure time was to 0.5 s to trace the path of the fluoresced light from the seeding particles. Fifty consecutive images were recorded in this fashion with a frame rate of 1.93 frames per second (fps). A recording of the flow field, using a 100 W halogen lamp light, was also carried out with an exposure time of 10 μs. Fifty images were taken at 12.36 fps.

Micro-PIV measurements were then taken with a time delay of 10 ms between each image. Fifty image pairs were recorded and analysed using VISIFLOW. The cross correlation interrogation regions were 128 × 128 pixels in size with a 75% overlap. The resulting vector spacing is 32 pixels or 51 μm. There were no vector interpolations or filtering carried out in the analysis. Lastly the velocity vectors were ensemble averaged over the fifty image pairs.

3.2. Bubble in a microchannel

A liquid drop in the microchannel was formed by placing one drop of DI water with seeding particles in one port and then applying gentle suction from the other port. An air bubble was trapped at each end of the channel, which were separated by the liquid slug (Figure 3). The length of the liquid slug was about 0.5 mm while the length of air bubble was about 0.375 mm. The PZT disk was placed on top of the microchannel and the edge of the disk was about 1~2 mm from the air bubble. The working solution contained 0.6 μm fluorescent particles. A sinusoidal excitation signal was applied by the generator to the PZT disk with a peak to peak voltage of 30 V and frequency of 9.98 kHz.

The smaller geometries of the microchannel were imaged using the 40× magnification objective. This permits the use of smaller seeding particles. The field of view provided by the 40× objective was 130 μm × 130 μm with a depth of field of 0.75 μm. Images were taken on a focal plane located at $z = 15$, 45 (mid-plane) and 75 μm, respectively. Only data at $z = 75$ μm were shown in the present paper. The same experimental techniques as in the first set were used to obtain streakline photographs, recorded movies and PIV measurements, however the time delay between laser pulses for PIV measurements was adjusted to 5 ms.

4. RESULTS

4.1. Bubble between two plane walls

On applying the excitation signal to the PZT disk, vigorous steady streaming was observed around the bubble. The flow is a uniform clockwise circulation centred on the bubble extending well beyond the oscillatory Stokes layer approximately 83 μm thick according to (1). The streamlines are shown in Figure 4. The length of the streamlines provides an indication of the relative magnitude of the velocities with longer streamlines indicating regions of higher velocity.

It is clear that the fluid circulates around the bubble, with a high velocity region near the bubble surface. This is confirmed by the velocity data from the PIV measurements (Figure 5). The maximum velocity near the bubble surface is in the order of 1 mm/s.
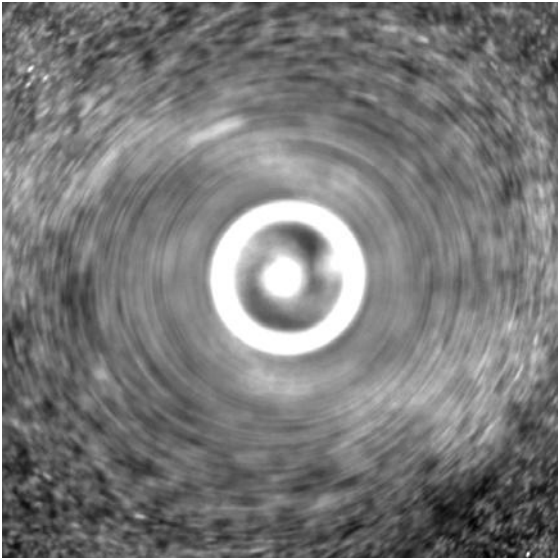

Figure 4: Streamlines depicting the steady circulation streaming flow about an oscillating bubble. Photos are taken by fluorescence of tracer microspheres with 532 nm light and the CCD exposed for 0.5 s.
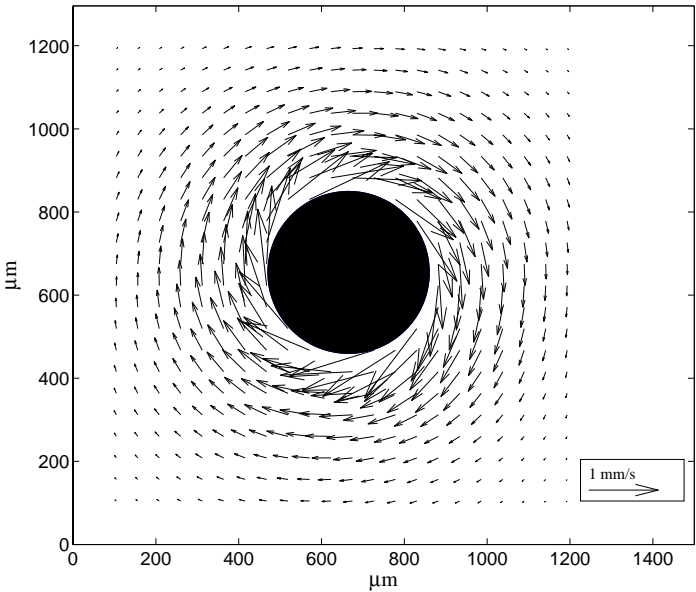

Figure 5: Micro-PIV determined velocity vectors around an oscillating bubble. Velocities of the order of 1 mm/s are observed near the bubble surface.

Figure 6 shows the distributions of radial component u_r, angular component u_θ and magnitude $|u|$ of velocity as a function of θ. These velocity profiles were extracted for $r = 400$ μm. For an ideal circular vortex, the radial velocity is zero and the only contribution to total velocity is the angular velocity component. Figure 6 shows that the radial component of the velocity is much smaller than the angular component. The angular velocity remains roughly constant at 350 μm/s while the radial velocity is close to zero, implying that the flow is approximately circular. Figure 7 shows the distributions of the velocity magnitude as a function of θ at $r = 300$, 350 and 400 μm, respectively. The results show the general trend of decreasing velocity with increased radial distance. The variation of the angular velocity component as a function of r is shown in Figure 8. The velocity increased from the bubble edge to a value of 0.85 mm/s at $r = 220$ μm and dropped rapidly as r increased.
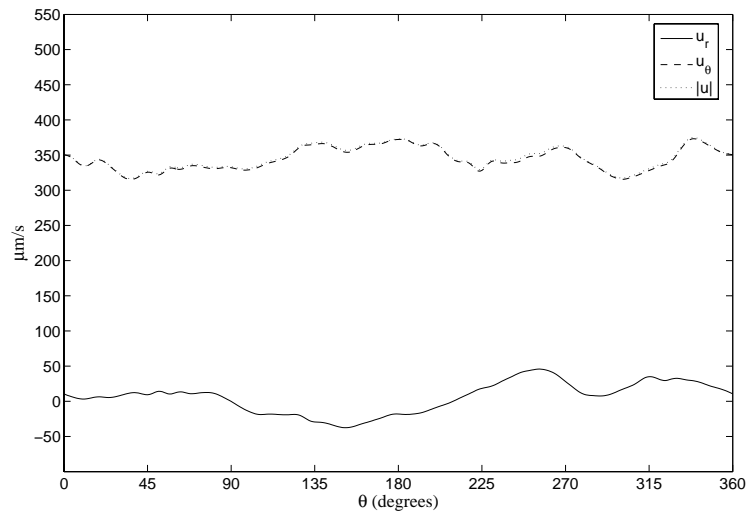

Figure 6: Velocity profiles of the variation in u_r, u_θ and $|u|$ with θ at a radial distance of 400 μm from the centre of the bubble. Radial velocity u_r is approximately zero.
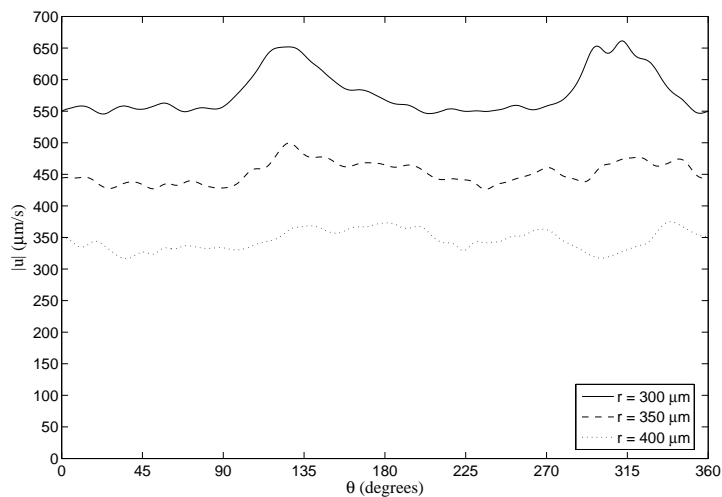

Figure 7: Distributions of velocity magnitude $|u|$ as a function of θ at $r =300$, 350 and 400 μm, respectively. r is measured from the bubble centre.
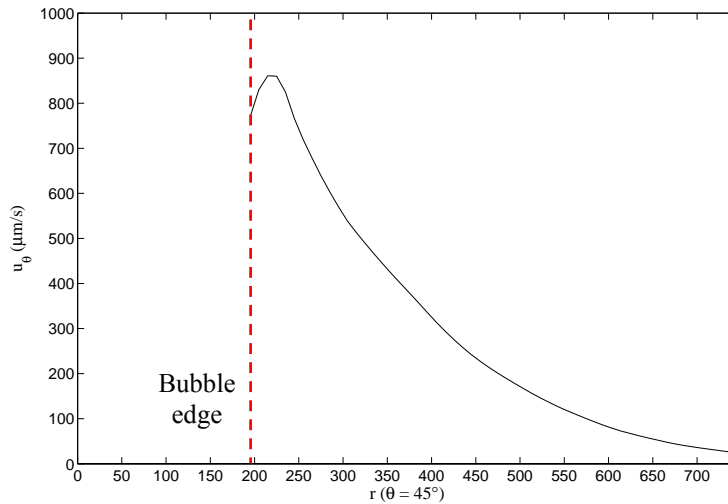
Figure 8: Distribution of the angular velocity component as a function of *r* at *θ* = 45 degree.

The use of low magnification and low numerical aperture objectives places a limit on the accuracy of the micro-PIV measurements. The depth of field of the objectives defines the image plane for analysis; however objectives with small numerical apertures and magnifications will deliver comparatively large depths of field with respect to microfluidic dimensions. The depth of field *δz* of these objectives estimated following Inoue and Spring[16] is defined as:

$$\delta z = \frac{n\lambda}{NA} + \frac{nd}{M \cdot NA} \tag{2}$$

Here *n* is defined as the refractive index of the fluid between the objective lens and the microfluidic device (n=1 for air), *d* is the smallest distance that can be resolved by a detector located in the image plane for a microscope (for a CCD camera this is the pixel size, 6.45 μm), *M* is the magnification of the optical system, *λ* is the wavelength of incident light (532 nm) and *NA* is the numerical aperture of the objective lens. Hence the depth of field for the 4× and 40× objectives are 16.6 μm and 1.2 μm respectively. This clearly shows the desirability of using high numerical aperture optics in micro-PIV measurements. The depth of field of the 4× objective is roughly 2.5% of the depth of the chamber. The large depth of field implies that the velocity in this first set of experiments was averaged over a large *z* distance.

4.2. Bubble in a microchannel

The flow field in the vicinity of the interface of the slug of air and the working fluid in the microchannel showed localized streaming upon acoustic excitation. The flow was clearly three dimensional as particles were moving in and out of focus in different regions of the image. Figure 9 shows the streamlines of the flow measured at *z* = 75 μm while Figure 10 shows the corresponding velocity vectors determined by the micro-PIV measurements. On the left side of the image is the edge of the interface with the majority of the slug of air out of view on the left side. Near this edge and extending about 70 μm along the length of the channel, there is significant streaming directed towards the interface. From the flow visualisation and PIV data, it seems reasonable to postulate that there was an anti-clockwise vortex near the interface in the vertical plane (Figure 11). Fluid was circulated from the top region towards the bubble and then towards the bottom region before being driven back. From the top view, the fluid was driven into the centre region near the bubble interface. The edge of vortex appeared to be at approximately *x* = 90 μm.
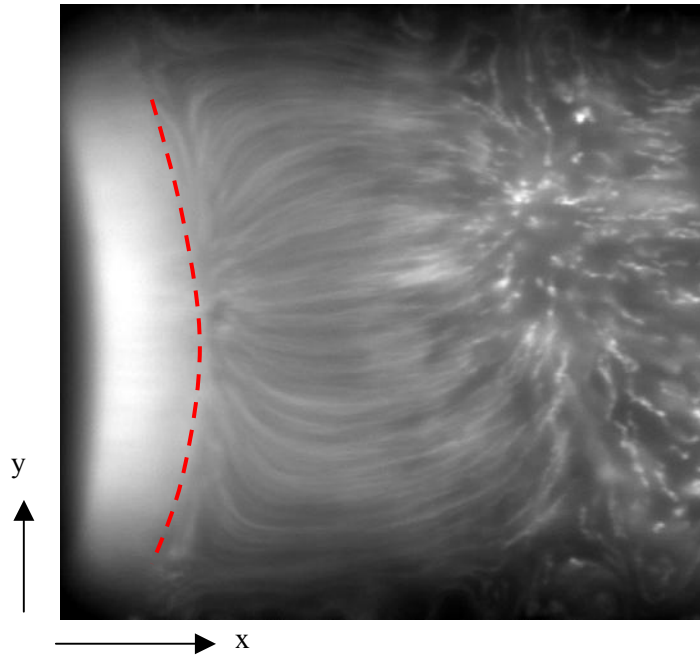
Figure 9: Streamlines depicting the steady streaming flow near the interface of an air slug and water in a microchannel at $z = 75\mu$m. The interface is indicated by the broken line. The interface edge is show on the left side with fluid moving towards the interface. Photos are taken by fluorescence of tracer microspheres with 532 nm light and the CCD exposed for 0.5 s.
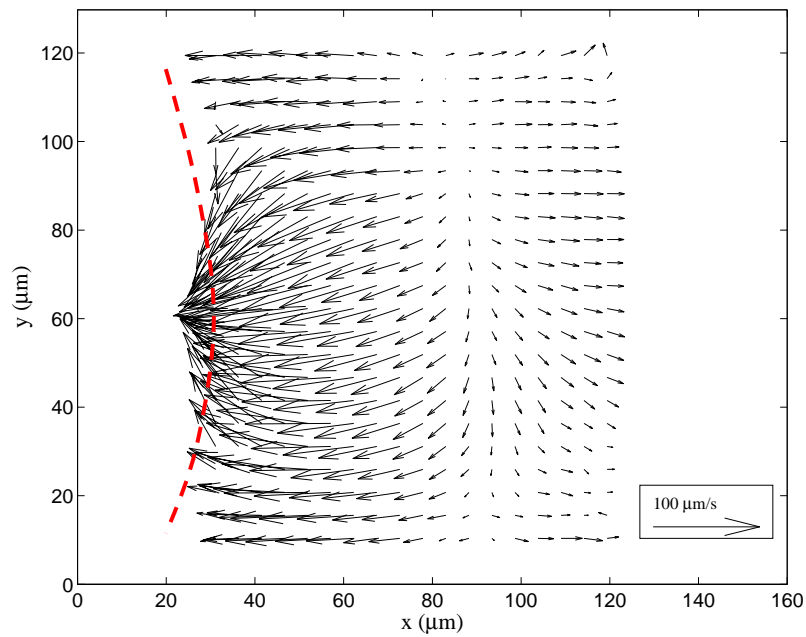

Figure 10: Micro-PIV determined velocity field of the air-water interface in a microchannel. Fluid is moving into the focal plane along $x = 90$ μm and away from the focal plane along $x = 20$ μm. The interface is indicated by the broken line.
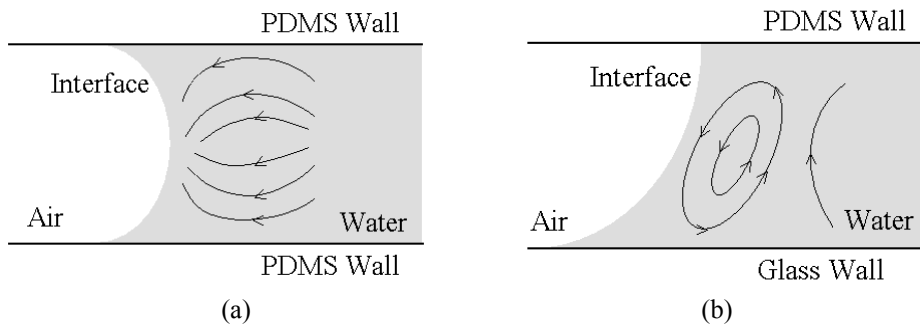
Figure 11 Streaming flow pattern near the air-water interface. (a) Top view, (b) Side view.

Figure 12 and Figure 13 show the distributions of velocity components u and v as a function of x, where u and v refer to the velocity components in the longitudinal (x) and transverse (y) directions, respectively (refer to Figure 3 for coordinate definitions). The origin of the coordinate, i.e. $x = 0$, was located 30μm to the left of the interface. The peak values of the longitudinal velocity component appeared at $x = 50 \sim 55$ μm, with the maximum value observed at the centreline. However, due to the converging behaviour in the xy-plane, the maximum magnitude of the transverse velocity component was observed at halfway between the centreline and the wall, e.g. $y = 30$ μm (Figure 12). Although there appears to be significant variation of the velocities along the channel, this may be deceptive as velocities in the direction normal to the image plane are not resolved.
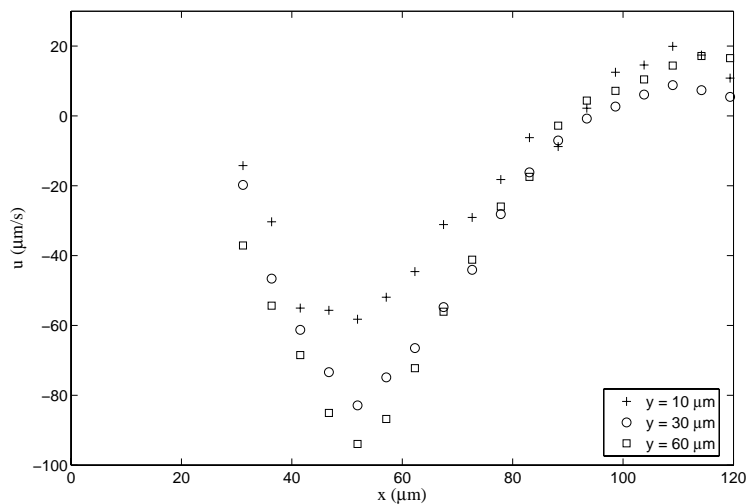

Figure 12: Distributions of the longitudinal velocity component u along the channel for y = 10, 30 and 60 μm, respectively.
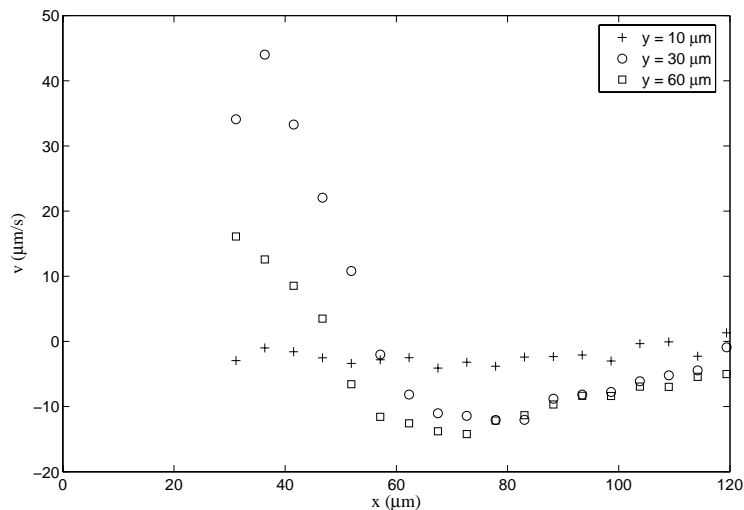
Figure 13: Distributions of the transverse velocity component *v* along the channel length along the channel for y = 10, 30 and 60 μm, respectively.

5. CONCLUSION

This paper presented micro-PIV measurements of the velocity fields around oscillating bubbles in microfluidic geometries. Excitation of the gas bubbles was achieved using a PZT disk. Acoustic microstreaming was demonstrated for a 195 μm radius bubble in water between two plane walls. The velocity vectors showing circulation around the bubble matched the streaklines imaged using fluorescent particles very well. The magnitude of the velocity was shown to decrease with distance from the bubble. The maximum velocity was found to be around 1 mm/s near the bubble surface. A second set of the PIV measurements wad carried out to measure the streaming at the interface of a trapped slug of air and water in a microchannel of 100 μm × 90 μm cross section. When the slug of air was excited the fluid showed strong three dimensional movement with fluid moving in a loop towards and away from the interface. The length of this loop was roughly 70 μm. Velocities in the order of 100 μm/s were observed near the water/air interface.

6. ACKNOWLEDGEMENTS

7. REFERENCES

1. R.H. Liu, J. Yang, R. Lenigk, J. Bonanno, P. Grodzinski, "Self-contained, fully integrated biochip for sample preparation, polymerase chain reaction amplification, and DNA microarray detection", Analytical Chemistry, 76, 7, 1824-1831, 2004
2. M.W. Losey, R.J. Jackman, S.L. Firebaugh, M.A. Schmidt, K.F. Jensen, "Design and fabrication of microfluidic devices for multiphase mixing and reaction", Journal of Microelectromechanical Systems, 11, 6, 709-717, 2002
3. S.J.Lee, A. Chang-Chien, S.W. Cha, R. O'Hayre, Y.I. Park, Y. Saito, F.B. Prinz, "Design and fabrication of a micro fuel cell array with "flip-flop" interconnection", Journal of Power Sources, 112, 410-418, 2002

4. I. Moser, G. Jobst, G.A. Urban, "Biosensor arrays for simultaneous measurement of glucose, lactate, glutamate, and glutamine" , Bionsensors and Bioelectronics, 17, 297-302, 2002

5. R.J. Adrian, "Particle –imaging techniques for experimental fluid mechanics", Annual Review of Fluid Mechanics, 23, 261-304, 1991

6. J. G. Santiago, S. T. Wereley, C. D. Meinhart, D. J. Beebe, R. J. Adrian, "A particle image velocimetry system for microfluidics", Experiments in Fluids 25, 316-319, 1998.

7. C. D. Meinhart, S. T. Wereley, J. G. Santiago, "PIV measurements of a microchannel flow", Experiments in Fluids, 27, 414-419, 1999.

8. S. Devasenathipathy, J.G. Santiago, S.T. Werely, C.D. Meinhart, K. Takehara, "Particle imaging techniques for microfabricated fluidic systems", Experiments in Fluids, 34, 504-514, 2003

9. C.D. Meinhart, H. Zhang, "The flow structure inside a microfabricated inkjet printhead", Journal of Microelectromechanical Systems, 9, 1, 67-75, 2000

10. B.J. Kim, Y.Z. Liu, H.J. Sung, "Micro PIV measurement of two-fluid flow with different refractive indices", Measurement Science and Technology, 15, 1097-1103, 2004

11. T.G. Leighton, *The Acoustic Bubble*, Academic Press, 1997

12. J. Kolb, W.L. Nyborg, "Small-scale acoustic streaming in liquids", The Journal of the Acoustical Society of America, 28, 6, 1237-1242, 1956

13. S.A. Elder, "Cavitation microstreaming", The Journal of the Acoustical Society of America, 31, 1, 54-64, 1959

14. P. Marmottant, S. Hilgenfeldt, "Controlled vesicle deformation and lysis by single oscillating bubbles", Nature, 423, 153-156, 2003

15. R.H. Liu, R. Lenigk, R.L. Druyor-Sanchez, J. Yang, P. Grodzinski, "Hyrbridization enhancement using cavitation microstreaming", Analytical Chemistry, 75, 1911-1917, 2003

16. S. Inoue, K.R. Spring, Video Microscopy: The Fundamentals, Plenum Publishing Corporation; 2nd edition, 1997.